Supporting Information

O'Gorman and Schneider 10.1073/pnas.0907610106

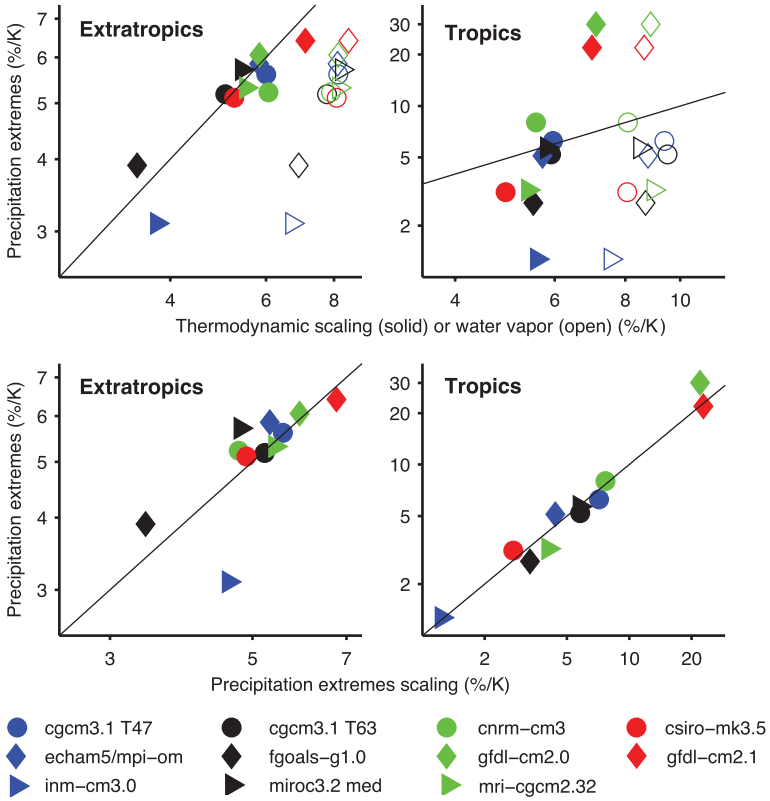

Fig. S1. As in Fig. 3, but with logarithmic axis scales.

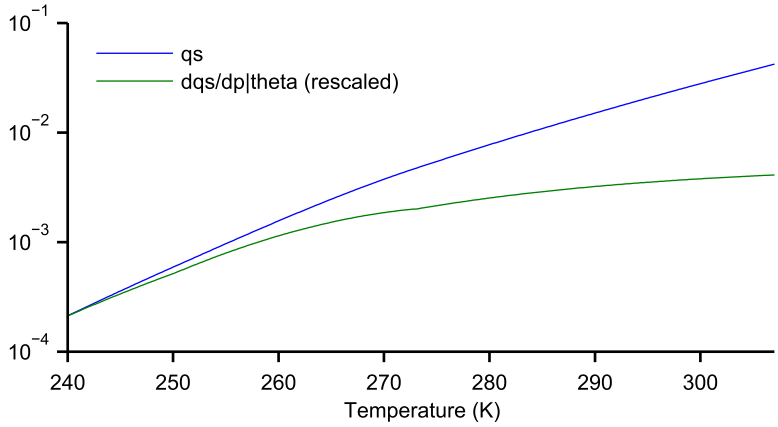

Fig. S2. Comparison of the dependence on temperature of the saturation specific humidity q_s (blue) and the (rescaled) moist-adiabatic derivative of saturation specific humidity $dq_s/dp|_{\theta^*}$ (green). For ease of comparison, the moist-adiabatic derivative was rescaled by a constant so that it numerically equals the saturation specific humidity at the lowest temperature shown (240 K). Both quantities are evaluated at a pressure of 800 hPa. A similar figure in ref. 8 differed from this one by using idealized moist thermodynamics to evaluate the saturation vapor pressure.

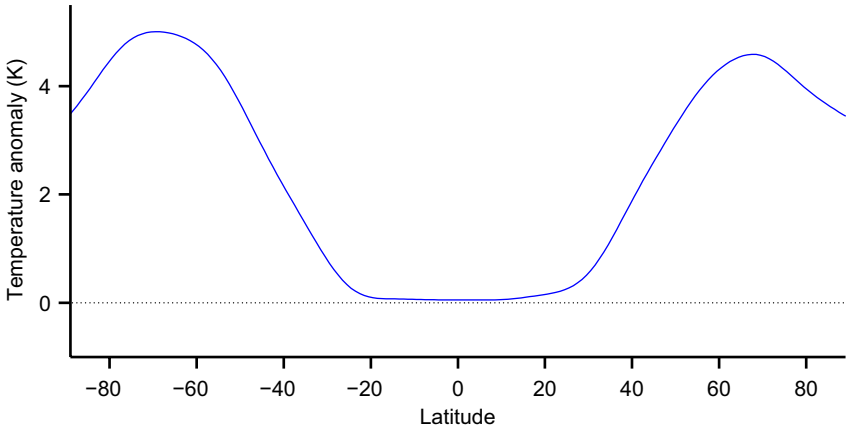

Fig. S3. Zonal-and time-mean temperature anomaly at 600 hPa conditioned on the 99.9th percentile of daily precipitation. The daily temperature anomaly at a given latitude, longitude, and level is defined relative to the monthly mean temperature there over the years 1997–2006. Precipitation data are from GPCP, and temperature data are from the NCEP2 reanalysis. The temperature data are given at a horizontal resolution of 2.5°, and because temperature fields are smoother than precipitation fields, we chose to linearly interpolate the temperature anomalies to the 1° grid of the precipitation data before calculating the conditional mean over the precipitation extremes.

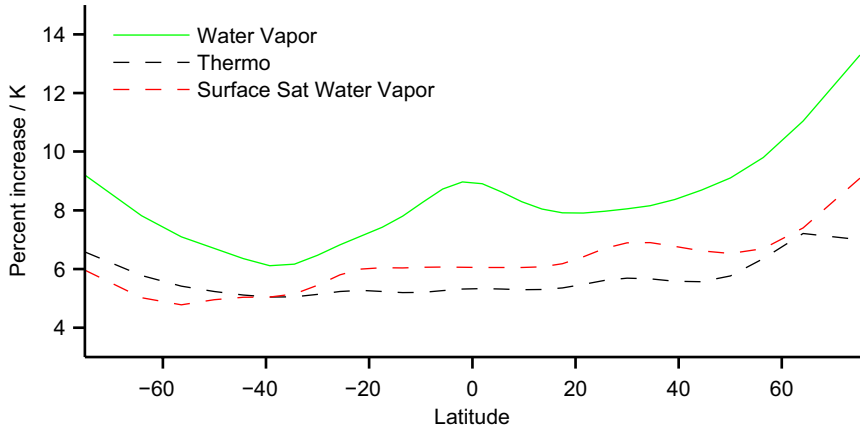

Fig. S4. Fractional changes in the zonally averaged atmospheric water vapor content (green), thermodynamic scaling for precipitation extremes (black dashed), and the saturation specific humidity calculated from the near-surface temperature when precipitation extremes occur (red dashed). The lines show multimodel medians of the fractional changes relative to the 20th century values, normalized by the global-mean change in surface air temperature for each model. The precipitation extreme considered is the 99.9th percentile of daily precipitation.

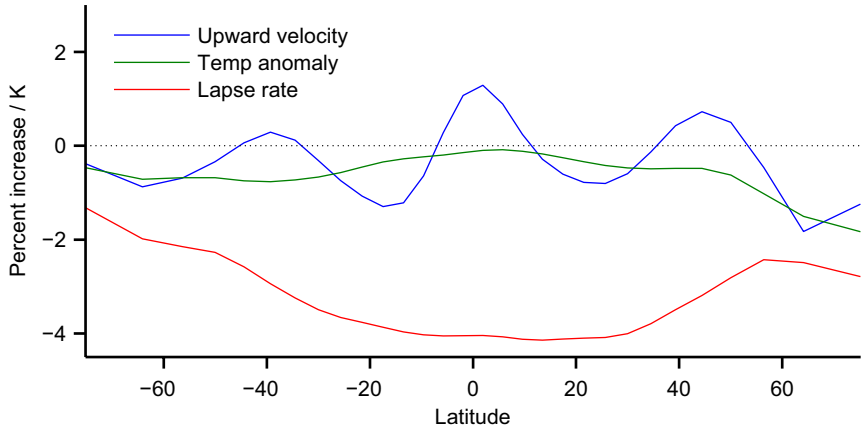

Fig. S5. Estimates of the contributions from different components of the precipitation extremes scaling to its change with climate for the 99.9th percentile of daily precipitation. Each line is the difference in the fractional change of the full scaling minus the fractional change in a simplified scaling. The simplified scalings in each case are: omitting the upward velocity (the thermodynamic scaling) (blue), neglecting the temperature anomaly when precipitation extremes occur by using the mean of the climatological monthly temperature averaged over longitudes and days when the precipitation extremes occur (green), and not accounting for changes in the moist-adiabatic lapse rate by using the dry-rather than moist-adiabatic derivative of saturation specific humidity (red). The differences shown are between the multimodel median of fractional changes in each scaling normalized by the change in global-mean surface air temperature for each model.

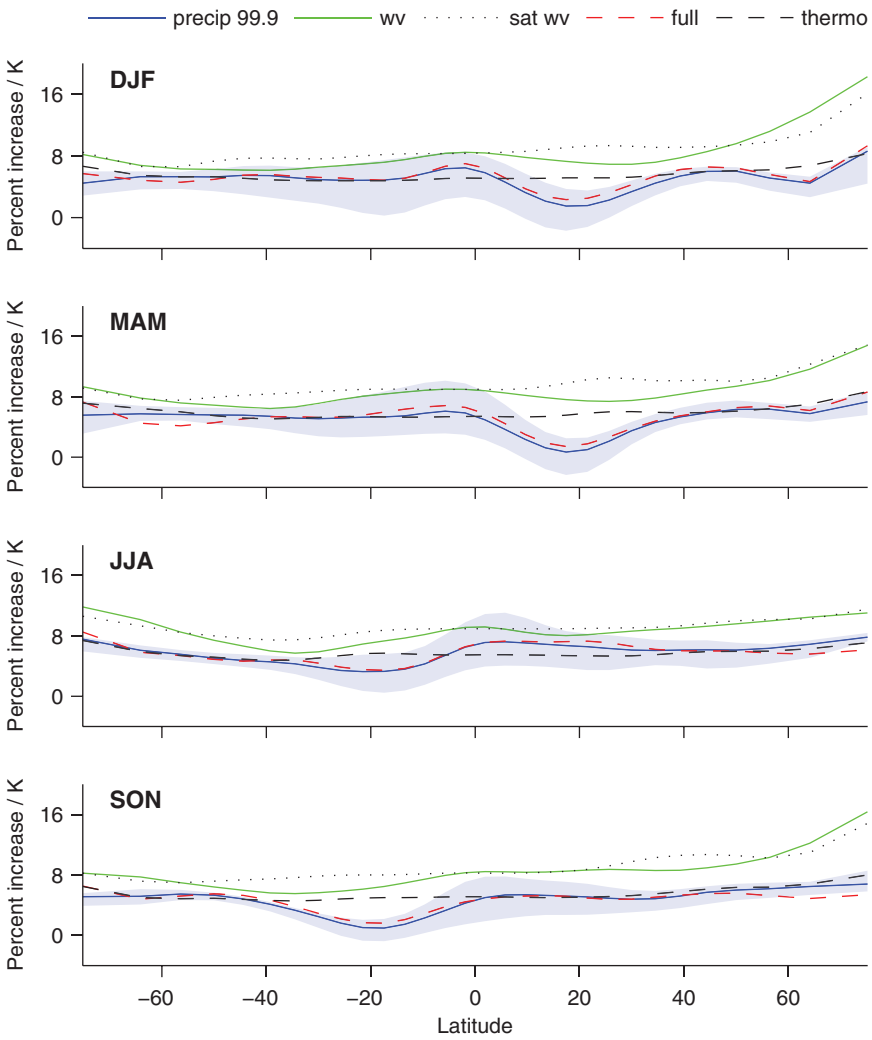

Fig. S6. As in Fig. 2, but for individual seasons: December/January/February (DJF), March/April/May (MAM), June/July/August (JJA), and September/October/November (SON).

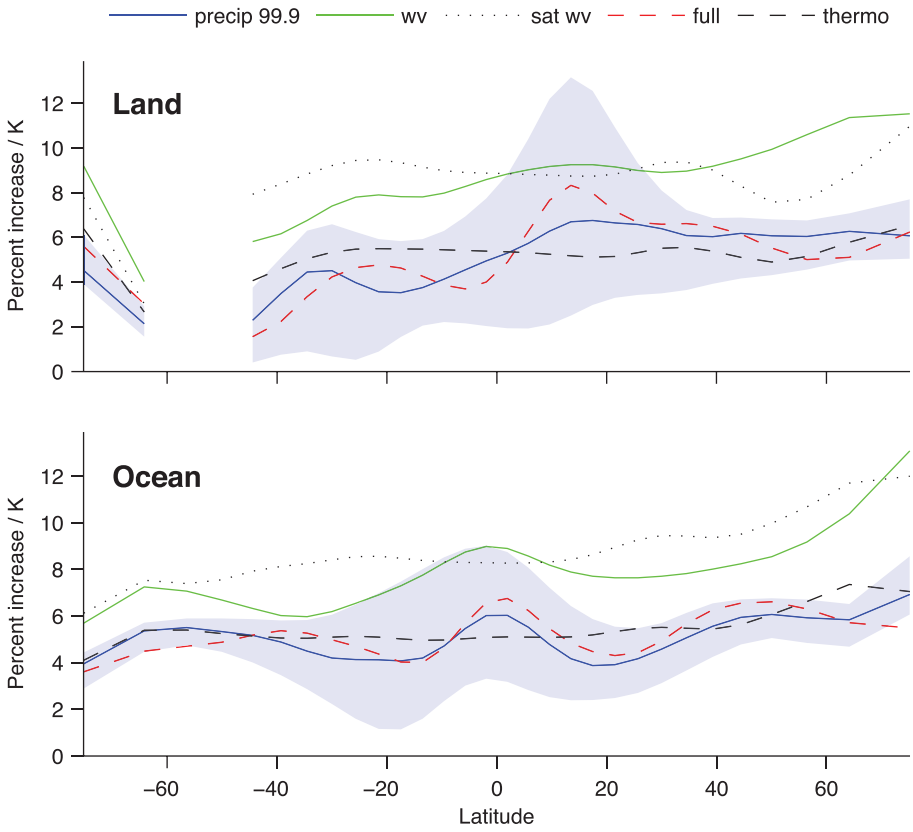

Fig. S7. As in Fig. 2, but considering statistics only over land (*Upper*) and only over oceans (*Lower*).

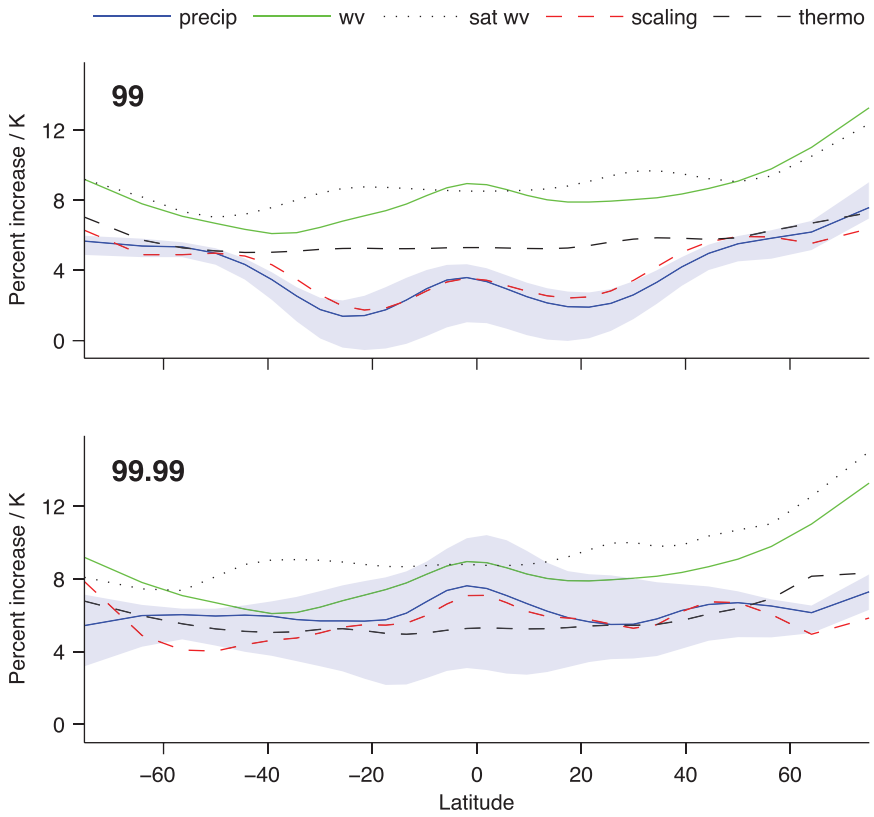

Fig. S8. As in Fig. 2, but for the 99th percentile (*Upper*) and the 99.99th percentile (*Lower*) of daily precipitation.